Scripta Materialia 150 (2018) 7–12

Contents lists available at ScienceDirect

Scripta Materialia

journal homepage: www.elsevier.com/locate/scriptamat

Regular article

# Characterization of novel high-speed die attachment method at 225 °C using submicrometer Ag-coated Cu particles

Chang Hyun Lee, Eun Byeol Choi, Jong-Hyun Lee *

*Department of Materials Science and Engineering, Seoul National University of Science and Technology, 232 Gongneung-ro, Nowon-gu, Seoul 01811, Republic of Korea*

ARTICLE INFO

*Article history:*
Received 2 February 2018
Received in revised form 19 February 2018
Accepted 19 February 2018
Available online xxxx

*Keywords:*
Sintering
Surface modification
Nanostructured materials
Electronic packaging
Bonding by silver dewetting

ABSTRACT

A novel die-attaching technology, using the in-situ dewetting of Ag shells in submicrometer Ag-coated Cu (Cu@Ag) particles during heating in air, was suggested for power device packaging. The particle size-dependent dewetting of Ag induced the formation of tiny nodules and rapid sinter bonding via fast Ag transfer under external pressure. A die attached by thermal compression for 5 min at 225 °C using 200- or 350-nm Cu@Ag particles showed shear strengths approaching or surpassing that (18.0 MPa) of a die attached using Pb-5Sb.



As hybrid and electronic vehicles gain prevalence, packaging technologies for high-heat power devices, such as insulated-gate bipolar transistors using Pb-free and low-cost bonding materials, have attracted increasing industrial interest [1–7]. In such applications, Si is increasingly replaced with wide-bandgap semiconductor materials, such as SiC and GaN, which operate with higher power densities and efficiencies at higher temperatures [8–11]. Hence, there have been many studies using wide-bandgap semiconductors to increase chip junction temperatures beyond 200 °C with bondlines indicating higher remelting points and thermal conductivities [1,5,6,12–20].

Regarding die-attachment processes and materials, soldering inevitably forms large voids that may cause severe degradation in thermal conductivity and reliability. Studies on the suitability of high-temperature Pb-free solder alloys retain problems inherent to soldering, such as high processing temperatures, low thermal conductivities, high cost, insufficient wettability, and poor corrosion resistance [21–24].

Transient liquid-phase (TLP) bonding and sinter bonding using Ag particles are the best available alternatives to soldering [25–28]. Despite the low material cost and the uniqueness of inducing a remelting point higher than the bonding temperature, TLP bonding possesses serious drawbacks including the brittle nature of the intermetallic compound (IMC) bondline and long bonding times at relatively high temperatures to form full IMC bondlines [25–28]. Therefore, more recent studies on alternative die-attachment technologies have focused on sinter bonding under external pressure >10 MPa, using pastes including Ag particles, which present high remelting point and thermal conductivity [12,15,16,19]. The development of processes with short sintering times, low sintering temperatures, and pressureless attachment is also important [12–14,16,20]. For example, since the Ag particle size significantly influences the sintering speed, much smaller Ag particles are used to increase the sintering speed [12,16]. Nevertheless, industrial sinter bonding using Ag particles is not common because of the inherently high material cost (which increases with decreasing size of Ag particles) and Ag migration.

Cu, which exhibits high electrical and thermal conductivities approaching those of Ag, is considered the best low-cost alternative material. However, the easy surface oxidation of Cu severely impairs its application as a bonding material [29–31]. These disadvantages can be overcome by converting or suppressing surface oxidation. For example, a low-pressure die attachment process using in-situ surface reduction of Cu particles during heating at 300 °C in formic acid vapor has been reported recently [5].

Here, a novel high-speed die attachment technology at 225 °C has been suggested, using the Cu-based particulate material Ag-coated Cu (Cu@Ag). The main parameters considered were the Cu@Ag core-shell structured particle sizes and bonding times.

Cu particles of three different sizes (200, 350, and 900 nm) were synthesized in house using a retained wet reduction method. The Cu particles were coated with 15 wt% Ag shells by electroless plating to yield sufficient coating coverage, though the average size of the core Cu particles was several hundreds of nanometers [32]; the shell thickness was varied from several to several tens of nanometers depending on the average sizes of the core particles.

The initial sizes and morphologies of the prepared Cu@Ag particles and morphological changes after heating in air were examined using

* Corresponding author.
*E-mail address:* pljh@snut.ac.kr (J.-H. Lee).

https://doi.org/10.1016/j.scriptamat.2018.02.029
1359-6462/

field-emission scanning electron microscopy (FE-SEM, JSM-6700F, JEOL Ltd.). Phase changes after heating in air were analyzed using X-ray diffraction studies (XRD, JP/MAX-3C, Rigaku Denki). To evaluate oxidation behavior, the weight changes of the Cu@Ag particles upon heating in air were measured by thermogravimetric analysis (Q600, TA Instruments, installed in KBSI PH407 Pusan) in both dynamic and isothermal heating modes.

Pastes containing the fabricated Cu@Ag particles were prepared by mixing with α-terpineol (98.5%, Samchun Chemical Co., Ltd.) as a vehicle with a particle-to-vehicle weight ratio of 85:15. Die attachment tests were performed using a dummy Si die of area $3 \times 3$ mm$^2$ and a Si substrate of area $10 \times 10$ mm$^2$ finished with Ag. The Ag finishes were formed by additional sputtering onto a Cu/Ti-metallized Si wafer. The prepared pastes were printed onto the Ag-finished substrates through a stencil mask with a slit volume of $5 \times 5 \times 0.1$ mm$^3$ using a squeegee. After printing, the die was aligned with the printed pattern and the sandwich-structured sample was heated to 225 °C at 50 °C/s. The die attachment was performed in air by pressing at 10 MPa throughout the bonding time. In some cases, preheating at 150 °C was applied for 5 min to evaporate the vehicle from the paste and the die was aligned after the preheating. The microstructures of the bondlines after pressing and shear fracture were observed using FE-SEM. The bonding strength of the bondline was defined as the maximum stress value measured during shear testing at 200 μm/s. To indirectly evaluate the electrical properties of the bondline containing only Cu@Ag particles, the sheet resistance of a Cu@Ag pellet was measured for different heating times. For pelletization, 0.5 g of Cu@Ag particles was poured into a mold cavity over a 15-mm-diameter bottom punch and pressed at 4900 N using the identical-diameter upper punch for 1 min. The sheet resistance was measured using a four-point probe linked to a source meter (2400, Keithley Instruments Inc.).

Fig. 1a–f shows the initial images of the Cu@Ag particles and the images obtained after heating at specific temperatures. The 900-nm Cu@Ag particles do not show any significant change in the surface until after heating at 200 °C; however, numerous tiny nodules are formed on the surface and the Cu@Ag particles are severely agglomerated upon heating at 250 °C [33]. This agglomeration is attributed to sintering among the Ag nodules formed via in-situ dewetting caused by the interfacial instability induced by the lattice difference of 11.7% between materials [34–36]. The 350-nm Cu@Ag particles (Fig. 1a–c) show many Ag nodules immediately after heating at 200 °C; particle agglomeration occurs at 250 °C. Meanwhile, Ag nodule formation and interparticle agglomeration occur throughout the 200-nm Cu@Ag particles upon heating at 200 °C (Fig. 1e). The agglomeration intensifies as the temperature is increased to 250 °C (Fig. 1f). These results imply that the in-situ Ag dewetting and interparticle agglomeration depend on the particle size after heating at identical temperatures.

In the XRD patterns (Fig. S1) obtained for the different Cu@Ag particles before and after heating at specific temperatures, the 900-nm particles show peaks attributed to only Cu and Ag even after heating at 200 and 225 °C, and a $Cu_2O$ phase is formed by Cu oxidation after heating at 250 °C. Based on the microstructure reported previously [33], oxidation was expected immediately after Ag dewetting. Meanwhile, the 350-nm particles show a small $Cu_2O$ (111) peak after heating at 225 °C, implying that dewetting and oxidation occur more quickly. With the 200-nm particles, a small $Cu_2O$ peak appears after heating at

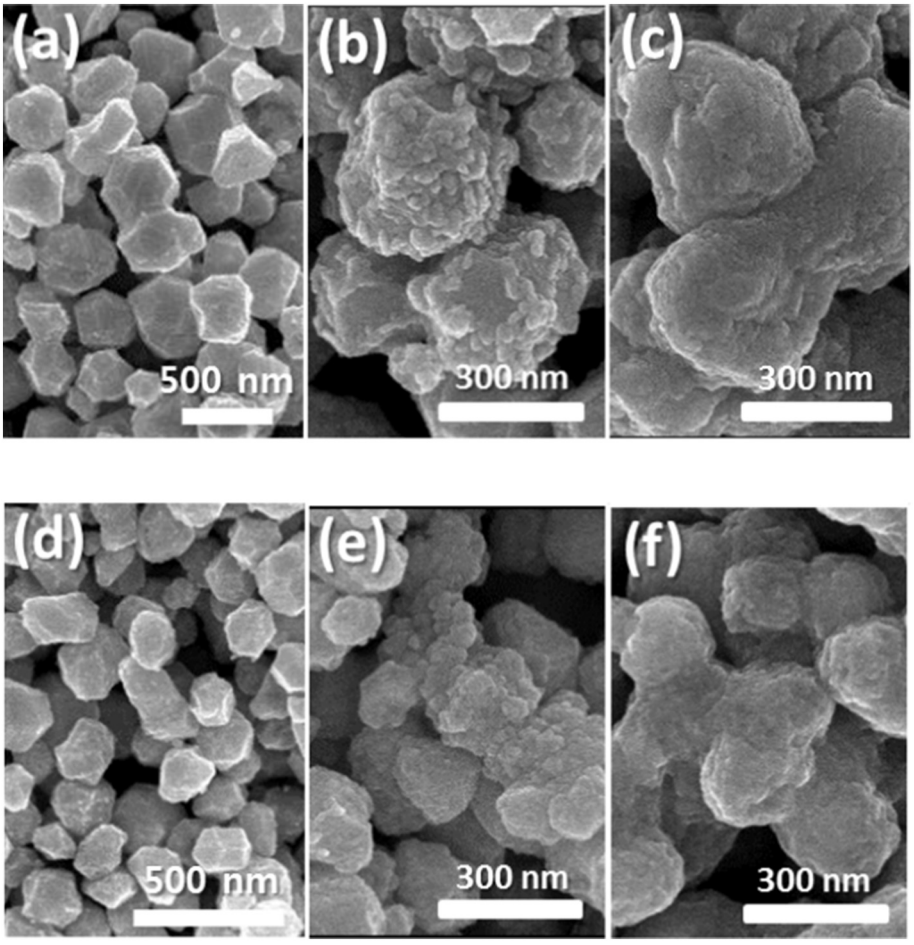


**Fig. 1.** (a, d) SEM images of initial Cu@Ag particles, and those of particles after heating to (b, e) 200 °C and (c, f) 250 °C. Different average particle sizes of (a, b, c) 350 nm and (d, e, f) 200 nm are shown.

200 °C. Therefore, Ag dewetting with different average particle sizes (Fig. 1) corresponds to variations in oxidation temperature as a function of the average particle size.

Fig. 2a shows the thermogravimetric results obtained for powders of different average sizes. All powders show slight decreases in weight until a certain temperature is reached, followed by steep increases with further increases in temperature. The slight weight decreases are attributed to the evaporation of organic components adsorbed on the prepared particle surfaces [37]. The steep weight gains are attributed to the formation of $Cu_2O$ by post-Ag-dewetting oxidation of the Cu cores [38]. The oxidation onset temperatures decrease upon reducing the average particle size from 900 to 200 nm: the onset temperatures for 200-, 350-, and 900-nm particles are 208.0, 213.6, and 242.0 °C, respectively. The order of occurrence of the oxidation in terms of particle size corresponded to that of dewetting observed in Fig. 1. The isothermal thermogravimetric results (Fig. 2b) also demonstrate the differences in the Ag shell stabilities for different particle sizes. The weight of the 200-nm Cu@Ag powder increases upon post-Ag-dewetting Cu oxidation after the evaporation of organic components during holding at 180 °C. Similar weight increase behavior occurs analogously in the 350-nm Cu@Ag powder, though the oxidation rate is decreased. However, the 900-nm Cu@Ag powder shows only continuous and slight weight loss due to evaporation of organic components, with no oxidation by dewetting occurring upon heat treatment for over 60 min. These results imply that the dewetting behavior is greatly influenced by the particle size. The decreased curvature radius in the smaller particles increases the areal interfacial energy between Ag and Cu, which induces more efficient dewetting; the reduction in dewetting onset temperature upon dynamic heating and dewetting proceeds at a higher rate in isothermal heating.

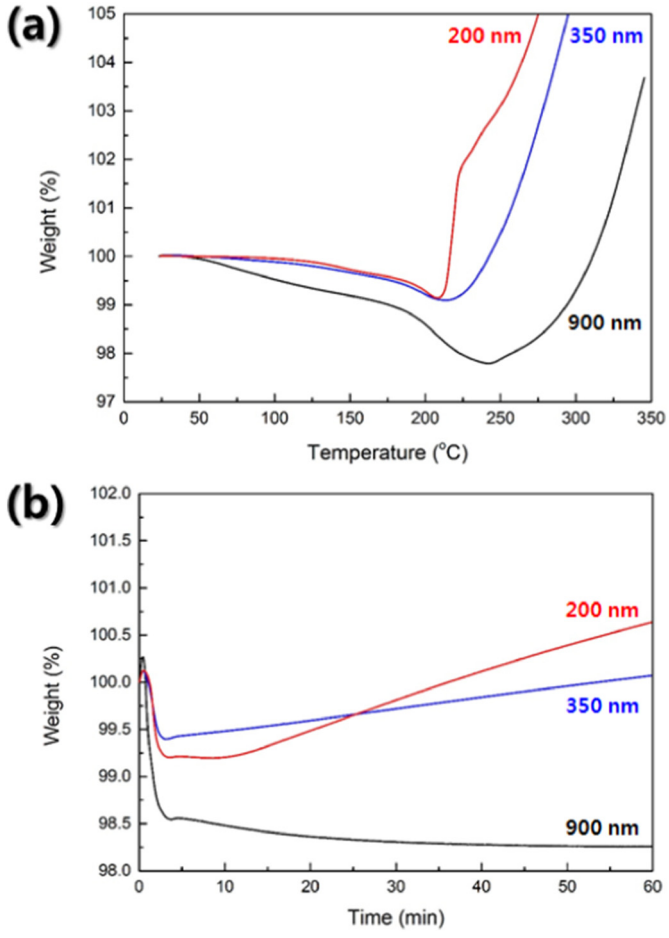


**Fig. 2.** Thermogravimetric analysis results of Cu@Ag particles having different average sizes measured in air during (a) dynamic heating at the heating rate of 10 °C/min and (b) isothermal heating at 180 °C.

Cross-sectional microstructures of bondlines sintered after 10-min bonding using the pastes containing Cu@Ag particles of different sizes are shown in Fig. 3a–c. In the 900-nm Cu@Ag particles (Fig. 3a), although the interfacial contact between particles indicates the occurrence of sintering, the bondline exhibits a porous structure with large interparticular voids, causing low compactness. However, the sintering rate between particles increased and the void size decreased with decreasing particle size; thus, the compactness and particle packing density of the bondline microstructure increased with decreasing particle size. Sinter bonding between Cu@Ag particles and the Ag-finished die and substrate is observed for all the samples.

The sinter bonding mechanism of the die is explained as follows. During heating, Ag dewetting occurs preferentially because of the interfacial energy induced by the significant lattice mismatch [34–36]. Since the interfacial energy depends on the curvature radius, dewetting occurs more readily on smaller particles. Ag in the top region of the nodule shapes formed by dewetting is transferred easily via transient quasi-fluid behavior by the size effect, such as melting-point depression by the Gibbs–Thomson effect [39–42] or nano-volcanic eruption [43]. Under intimate contact with neighboring particles, aided by external pressure, the surface transfer in the Ag shells rapidly induces necking between the core–shell particles. Sinter bonding between the Ag shell and Ag finish occurs in the same manner. Since the volume of the Ag shell cannot fill the total void volume, the density of the sintered bondline decreases with increasing particle size. However, the rapid Ag transfer in the shells induces fast sintering behavior. With increased bonding time, Ag necking is enhanced and becomes more widespread. As the bonding temperature approaches 250 °C, necking by Ag is followed by Cu necking [44].

The shear strengths of dies attached with different bonding times at 225 °C using the differently sized particles are shown in Fig. 3d. Preheating is applied in some cases to remove the vehicle in the paste before sinter bonding. While the strength increases with increasing bonding time for all Cu@Ag particle sizes because the degree of sintering is enhanced with increasing time, the bondline comprising the 900-nm particles shows low strength because of its low density (Fig. 3a). However, the bondlines fabricated using 200-nm particles show much higher strengths with enhanced density. The preheating step increases the shear strength. The bondline strengths achieved with bonding time of 3 min and 200- and 350-nm particles are relatively high. After 5 min, the preheated bondline strength obtained using 350-nm particles approaches that of a die attached using Pb-5Sb solder (18.0 MPa) [45]. The preheated bondlines made using 200-nm particles show the maximum strength of 19.5 MPa, surpassing that of Pb-5Sb. With additional bonding for up to 10 min, the strength achieved by sinter bonding using the 350- and 200-nm particles increase slightly. Preheating is thus helpful in increasing the bonding strength. Outgassing from the evaporation of the vehicle during preheating may hinder sintering and reduce the bondline strength, as observed in a similar die attachment experiment using a paste [46]. Hence, chip attachment may be best implemented such that sinter bonding initiates after outgassing terminates. Although the bondlines fabricated with 200-nm particles show the highest strengths, they are not greatly enhanced compared to those made using 350-nm particles. Therefore, while increasing compactness of the bondline microstructure increases the strength, an increase in interparticle interface area may compromise the increase in strength.

Fractured surfaces after shear testing for bonding times of 10 min for each particle size are presented in Fig. 4a–c. The fractured surface is located within the bondline for all samples, implying that the bonding at the Cu@Ag particles/Ag finish interface is more robust than that between Cu@Ag particles. Thus, the microstructures of the fractured surfaces reflect the porosity and density of the bondline. The fractured bondline comprising 900-nm particles shows large pores formed by the non-uniform particle distribution and small voids formed between

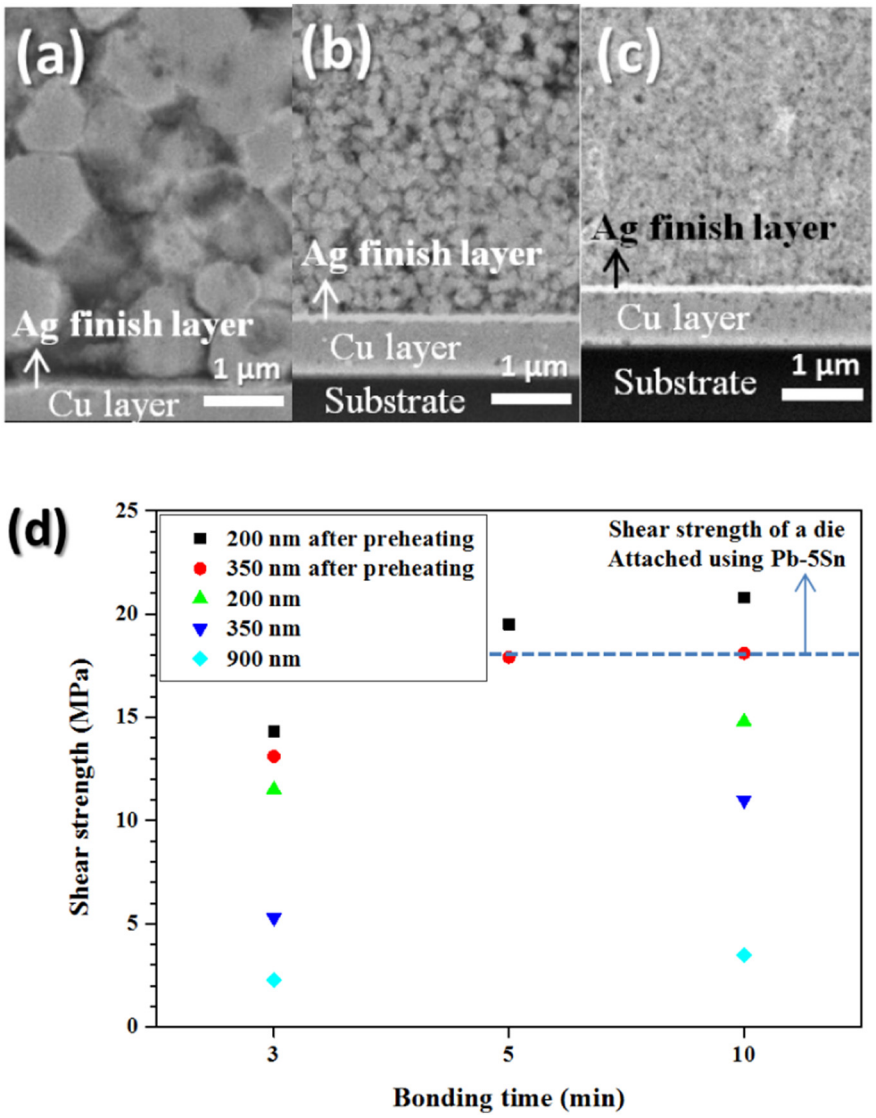


**Fig. 3.** (a, b, c) High-magnification cross-sectional SEM images of bondlines fabricated at 225 °C for 10 min with different particle sizes, and (d) shear strengths of dies bonded at 225 °C as functions of particle size and bonding time.

particles by incomplete sintering. Although the microstructural characteristics are identical, the sizes of pores and voids are significantly decreased with decreasing average particle size (Fig. 4b–c). In particular, the fractured bondline comprising 200-nm particles shows a compact microstructure with very small pores and voids.

Fig. 4d shows the changes in sheet resistivities in compacted pellets heated in air as functions of the average particle size, sintering temperature, and time. The resistance is measured at the bottom surface of a pellet in contact with the surface of a hot plate. The resistance is influenced mainly by the degree of interparticle sintering and oxidation [47]. In the pellet comprising 200-nm particles, the resistance increases continuously with increasing heating time at temperatures of 225 and 250 °C, indicating that the oxidation degree of the particles increases consistently with time. However, the resistance increases dramatically after 10 min due to the rapid oxidation behavior in the pellet heated at 250 °C, unlike that heated at 225 °C. A continuous but steeper increase is observed in the pellet comprising 350-nm particles during heating at 250 °C, induced by the combination of high oxidation rate and resultant low sintering rate. Meanwhile, the resistance increases slightly for the first 7 min and decreases slowly after 10 min during heating at 225 °C because the degree of sintering surpasses the degree of oxidation. These results indicate that heating at 250 °C in air oxidizes the Cu@Ag particles regardless of size, while oxidation at 225 °C depends strongly on the particle size.

In summary, a novel die-attachment method using the in-situ dewetting of Ag shell in submicrometer Cu@Ag particles during heating in air was successfully demonstrated. Smaller particle sizes showed quicker dewetting and oxidation. The Ag shell was transformed into small nodules by the dewetting and sinter bonding between particles proceeded rapidly through fast Ag transfer from the top regions of the nodules, aided by the applied external pressure. Since the dewetting and void size were strongly dependent on the particle size, the bondlines fabricated using particles of sizes 200 and 350 nm showed denser microstructures and higher bonding strengths. Dies attached by thermal compression at 225 °C for 5 min using both these particle sizes showed shear strengths approaching or surpassing that of a die attached using Pb-5Sb solder. Moreover, the heating conditions did not induce severe oxidation in the 350-nm particles. This facile die-attachment method could overcome the limitations of attachment methods using pure Ag particles; it may permit power device attachment at high speed, suitable bonding temperatures, and low material cost.

Supplementary data to this article can be found online at https://doi.org/10.1016/j.scriptamat.2018.02.029.

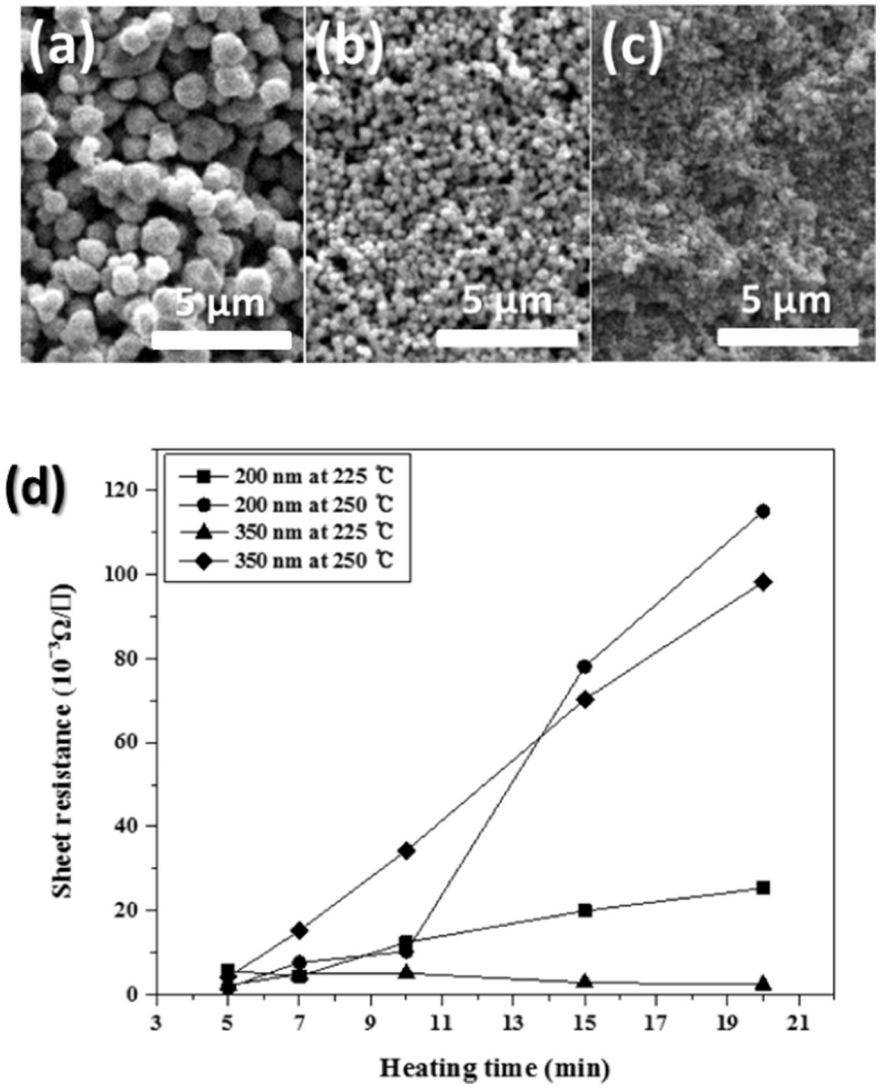


**Fig. 4.** (a–c) SEM images of the fractured surfaces after shear testing and (d) sheet resistivity values of pellets comprising particles of different average sizes heated in air with different sintering temperatures and times.

## Acknowledgments

This work was supported by the Materials & Components Technology Development Program (10080187) funded by the Ministry of Trade, Industry & Energy (MI, Korea). The authors also thank the Korean Basic Science Institute (KBSI), Busan Center for the thermogravimetric analysis.

## References

[1] J. Yan, G. Zou, Y. Zhang, J. Li, L. Liu, A. Wu, Y.N. Zhou, Mater. Trans. 54 (2013) 879.
[2] S.W. Park, S. Nagao, Y. Kato, H. Ishino, K. Sugiura, K. Tsuruta, K. Suganuma, J. Alloys Compd. 637 (2015) 143.
[3] T. Hu, H. Chen, M. Li, Mater. Des. 108 (2016) 383.
[4] X. Liu, S. He, H. Nishikawa, Scr. Mater. 110 (2016) 101.
[5] X. Liu, H. Nishikawa, Scr. Mater. 120 (2016) 80.
[6] J. Liu, H. Chen, H. Ji, M. Li, ACS Appl. Mater. Interfaces 8 (2016) 33289.
[7] X. Liu, S. He, H. Nishikawa, J. Alloys Compd. 695 (2017) 2165.
[8] H.S. Chin, K.Y. Cheong, A.B. Ismail, Metall. Mater. Trans. B Process Metall. Mater. Process. Sci. 41 (2010) 824.
[9] A. Drevin-Bazin, F. Lacroix, J.F. Barbot, J. Electron. Mater. 43 (2014) 695.
[10] D. Liu, D. Francis, F. Faili, C. Middleton, J. Anaya, J.W. Pomeroy, D.J. Twitchen, M. Kuball, Scr. Mater. 128 (2017) 57.
[11] L. Ceccarelli, P.D. Reigosa, F. Iannuzzo, F. Blaabjerg, Microelectron. Reliab. 272 (2017) 76–77.
[12] E. Id, S. Angata, A. Hirose, K.F. Kobayashi, Acta Mater. 53 (2005) 2385.
[13] K. Suganuma, S. Sakamoto, N. Kagami, D. Wakuda, K.-S. Kim, M. Nogi, Microelectron. Reliab. 52 (2012) 375.
[14] J. Yan, G. Zou, A. Wu, J. Ren, J. Yan, A. Hu, Y. Zhou, Scr. Mater. 66 (2012) 582.
[15] S. Soichi, K. Suganuma, IEEE Trans. Compon. Packag. Technol. 3 (2013) 923.
[16] S. Fu, Y. Mei, G.-Q. Lu, X. Li, G. Chen, X. Chen, Mater. Lett. 128 (2014) 42.
[17] T. Kunimune, M. Kuramoto, S. Ogawa, T. Sugahara, S. Nagao, K. Suganuma, Acta Mater. 89 (2015) 133.
[18] M.-S. Kim, H. Nishikawa, Mater. Sci. Eng. A 645 (2015) 264.
[19] S.A. Paknejad, A. Mansourian, J. Greenberg, K. Khtatba, L.V. Parijs, S.H. Mannan, Microelectron. Reliab. 63 (2016) 125.
[20] H. Zhang, Y. Gao, J. Jiu, K. Suganuma, J. Alloys Compd. 696 (2017) 123.
[21] K. Suganuma, K. Kim, J. Mater. Sci. Mater. Electron. 18 (2006) 121.
[22] Y.C. Liu, J.W.R. Teo, S.K. Tung, K.H. Lam, J. Alloys Compd. 448 (2008) 340.
[23] V. Chidambaram, J.J. Hattel, J. Hald, Microelectron. Eng. 88 (2011) 981.
[24] G. Zeng, S. McDonald, K. Nogita, Microelectron. Reliab. 52 (2012) 582.
[25] N.S. Bosco, F.W. Zok, Acta Mater. 52 (2004) 2965.
[26] J.F. Li, P.A. Agyakwa, C.M. Johnson, Acta Mater. 59 (2011) 1198.
[27] F.Q. Lang, H. Yamaguchi, H. Nakagawa, H. Sato, J. Electrochem. Soc. 160 (2013) D315.
[28] H. Feng, J. Huang, J. Yang, S. Zhou, R. Zhang, S. Chen, J. Electron. Mater. 46 (2017) 4152.
[29] W. Li, M. Chen, J. Wei, W. Li, C. You, J. Nanopart. Res. 15 (2013) 1949.
[30] Y.H. Kim, D.K. Lee, B.G. Jo, J.H. Jeong, Y.S. Kang, Colloids Surf. A Physicochem. Eng. Asp. 284 (2006) 364.
[31] X. Xu, X. Luo, H. Zhuang, W. Li, B. Zhang, Mater. Lett. 57 (2003) 3987.
[32] E.B. Choi, J.-H. Lee, Arch. Metall. Mater. 62 (2017) 1137.
[33] C.H. Lee, J.-H. Lee, Nanosci. Nanotechnol. Lett. 9 (2017) 1271.
[34] M. Grouchko, A. Kamyshny, S. Magdassi, J. Mater. Chem. 19 (2009) 3057.
[35] A. Muzikansky, P. Nanikashvili, J. Grinblat, D. Zitoun, J. Phys. Chem. C 117 (2013) 3093.
[36] C.-H. Tsai, S.-Y. Chen, J.-M. Song, I.-G. Chen, H.-Y. Lee, Corros. Sci. 74 (2013) 123.
[37] E.B. Choi, J.-H. Lee, Appl. Surf. Sci. 415 (2017) 67.
[38] H.T. Hai, H. Takamura, J. Koike, J. Alloys Compd. 564 (2013) 71.

[39] M. Takagi, J. Phys. Soc. Jpn. 9 (1954) 359.
[40] P.R. Couchman, W.A. Jesser, Nature 269 (1977) 481.
[41] G.L. Allen, R.A. Bayles, W.W. Jesser, Thin Solid Films 144 (1986) 297.
[42] T. Liang, D. Zhou, Z. Wu, P. Shi, Nanotechnology 28 (2017) 485704.
[43] S. Lin, S. Nagao, E. Yokoi, C. Oh, H. Zhang, Y. Liu, S. Lin, K. Suganuma, Sci. Rep. 6 (2016) 34769.
[44] X. Yu, J. Li, T. Shi, C. Cheng, G. Liao, J. Fan, T. Li, Z. Tang, J. Alloys Compd. 724 (2017) 365.
[45] E. Id, A. Hirose, K.F. Kobayashi, Mater. Trans. 47 (2006) 211.
[46] K. Xiao, K.D.T. Ngo, G.-Q. Lu, J. Mater. Res. 29 (2014) 1006.
[47] E.B. Choi, J.-H. Lee, J. Alloys Compd. 689 (2016) 952.